Colloids and Surfaces B: Biointerfaces 174 (2019) 367–373

Contents lists available at ScienceDirect

Colloids and Surfaces B: Biointerfaces

journal homepage: www.elsevier.com/locate/colsurfb

Protocols

On the effect of ligand shell heterogeneity on nanoparticle/protein binding thermodynamics

Ahmet Bekdemir[a], Suiyang Liao[a], Francesco Stellacci[a,b,*]

[a] Institute of Materials, École Polytechnique Fédérale de Lausanne (EPFL), Switzerland
[b] Interfaculty Institute of Bioengineering, EPFL, Switzerland

ARTICLE INFO

Keywords:
Nanoparticle-protein interactions
Analytical ultracentrifugation
Gold nanoparticles

ABSTRACT

Nonspecific protein adhesion to nanoparticle (NP) has been proven to have important implications in nanomedicine. However, there are only a few examples of careful studies relating protein binding thermodynamics to NP physicochemical features. In particular, a systematic investigation of how NP/protein binding parameters scale with size for sub-10 nm NPs and whether this scaling is affected by the surface feature of NPs remain unaddressed. Previously, we have developed an analytical ultracentrifugation (AUC) based method to determine NP/protein binding thermodynamic parameters that was shown to be particularly effective for sub-10 nm NPs. In this work, we exclusively utilize this method to investigate the binding parameters for a well-defined set of gold NPs with varying size and surface ligand ratios to the model protein human serum albumin. We find that gold NPs with a homogenous distribution of hydrophilic molecules in their ligand shell have a monotonic dependence of their binding constants and of the maximum number of bound proteins as a function of their surface area. On the other hand, a more complex relation is found for particles with patchy ligand shell. The findings of this research highlight the significance of surface morphology on the interplay between protein binding behavior and NP size.

1. Introduction

The adsorption of proteins on nanomaterials upon contact in biological media, called protein corona, has been center of an increasing interest in nanomedicine and nanotoxicology [1–3]. Because surface adsorbed proteins can alter or even hinder the designated biological functions of nanoparticles (NPs), the protein corona has been extensively studied *in vitro* and *in vivo* [4–6]. Over the last decade, physicochemical properties of NPs such as size, chemical composition, shape, charge and hydrophobicity have been shown to influence protein – nanoparticle interactions to a varying extent [4,7–10]. Hofmann and co-workers, for instance, carried out detailed investigations on iron-oxide nanoparticles and the effects of their surface charge and chemical structure on the protein corona composition with magnetic separation method [11–14]. Another study demonstrated that the number of proteins bound to nanoparticle surface is strictly size dependent while binding affinity is influenced in a more complex way [15]. In addition, the degree of surface hydrophobicity of PNIPAM:BAM hybrid nanoparticles was shown to influence the binding stoichiometry at least for human serum albumin [16]. However, these studies were typically focused on hundreds of nanometer sized NPs where proteins see the surface of nanoparticle almost like a flat surface. Apart from some works with single-sized nanoparticles [17,18], there is a lack of systematic study for the effect of size on the protein binding particularly at sub-10 nm level. It is crucial to note that when particle size is commensurate with serum proteins, the NP-protein interactions are expected to become different. First of all, only a few proteins can fit on a single particle thus crowding effect is more emphasized. Furthermore, when particles are smaller than 10 nm, the inhomogeneity on the surface in terms of topography and ligand morphology is expected to be small compared to the size of proteins (for simple geometrical reasons). We have shown that the phase separation of binary ligand mixtures on gold NPs into stripe-like domains [19,20] determines a number of interesting biological properties, including protein non-specific adsorption [21,22]. The question of how the presence of binary ligand mixture on the surface of sub-10 nm NPs affects the thermodynamic parameters in protein binding has not been addressed so far.

One important reason why there is a lack of such study is that investigating protein interactions of small NPs (less than 10 nm) has a number of methodological challenges. Data analysis is mostly complicated because the signal (fluorescence or scattering) that comes from NP/protein conjugates is affected by the background signals of either

* Corresponding author at: Institute of Materials, École Polytechnique Fédérale de Lausanne (EPFL), Switzerland.
E-mail address: francesco.stellacci@epfl.ch (F. Stellacci).

https://doi.org/10.1016/j.colsurfb.2018.11.027
Received 18 August 2018; Received in revised form 7 November 2018; Accepted 12 November 2018
Available online 14 November 2018

unbound/untagged proteins or inadvertent aggregates [23,24]. Recently we showed that analytical ultracentrifugation (AUC) could be one way to address these challenges as it allowed to investigate protein interactions of as small as 2.2 nm gold NPs [23]. Because AUC relies solely on sedimentation behavior of NPs that are gradually retarded upon protein adsorption on the surface, this method was shown to be effective without the need of any labelling neither NPs nor proteins. Our mathematical model described a Langmuir-adsorption-like change in the sedimentation coefficient of NP/protein conjugate as a function of the number of protein bound accurately and robustly. Fitting the experimental data to this model allowed us to calculate multitude of thermodynamic parameters of the interaction such as binding affinity (K_D), stoichiometry (N_{max}) as well as the cooperativity factor (Hill coefficient).

Here, we utilize this method to carry out a systematic study of small NP-protein interactions as a function of NP size and discuss how surface morphology influence this function. First, we report the design and synthesis of highly monodisperse gold NPs with 4 different sizes and surface coatings (fully charged hydrophilic, mixture of hydrophilic and hydrophobic and purely ethylene glycol). Then, we calculate binding parameters of these NPs against our model protein human serum albumin (HSA) and investigate their scaling with the size of NPs. Our results suggest a linearity between the surface area of hydrophilic gold NPs and their interaction with HSA, indicated with K_D and N_{max} values. The presence of binary ligands on the NPs surface, on the other hand, slightly distorts this linearity for binding affinity while radically removing for N_{max} values. This nonmonotonic behavior of binding stoichiometry as a function of size implies that surface morphology either affects the binding geometry or simply decreasing the binding regions on NP surface. Finally, we also have shown that size effect could be insignificant for other surface chemistries such as ethylene glycol units as they are resistant to HSA attachment at least for sub-10 nm gold NPs even at the physiological concentration of HSA.

2. Materials and methods

2.1. Materials

Chloro(triphenylphosphine)gold(I) (> 99.9% trace metals basis purity), 1-octanethiol (> 98.5% purity), borane tert-butylamine complex (powder, 97% purity) were purchased from Sigma Aldrich and used without further purification. HS-EG5-OH (EG5) ligand was purchased from PurePEG® and purged Argon after each use. 11-mercaptoundecane sulfonate, sodium salt (MUS) ligand was synthesized in-house according to previously reported protocol [25]. Human serum albumin (lyophilized powder, 97% purity) was obtained from Sigma Aldrich and used as is. All solvents were used ACS grade, straight out of the bottle without further purification. Analytical ultracentrifugation (AUC) experiments were carried out in Beckman Coulter ProteomeLab XLA/XLI ultracentrifuge with AnTi 50 and AnTi 60 rotors. Cell compartments such as aluminum cell covers, Epon® centerpieces and sapphire windows were purchased from SpinAnalytical.

2.2. 1-octanethiol (OT) gold nanoparticle synthesis

164 mg Chloro(triphenylphosphine)gold(I) and 20 μL 1-octanethiol were dissolved in solvent mixture (32 mL) at room temperature. In a separate vial, 200 mg borane tert-butylamine complex was dissolved in the same solvent mixture (32 mL) and put into the previous solution at room temperature. Solvent conditions and reaction temperature were varied in each synthesis to obtain different size for NPs which were summarized in Table 1. Right after mixing the reducing agent, the solution was immersed into heating bath of certain temperature and allowed to stir for 1.5 h. The reaction was then slowly cooled down to room temperature again followed by addition of methanol (around 50 mL). This resulted in precipitation of nanoparticles from the reaction solution. In order to collect nanoparticles, the solution was transferred to 50 mL centrifuge tubes and spun at 5000 g for 15 min. The centrifuge tube was refilled with methanol and mixed thoroughly before precipitating through centrifugation at 5000 g for 15 min. This refilling protocol was repeated at least 4 times to make sure all the starting materials were washed out of the solution. Finally, the pelleted nanoparticles were put under vacuum overnight to obtain dry powder OT coated gold nanoparticles.

Table 1
Experimental parameters for monodisperse OT coated gold NPs synthesis. Variation of solvent polarity and/or reaction temperature result different size of NPs without changing the core nature of the reaction (*e.g.* reactants, reducing agents, *etc.*).

	OT(1)	OT(2)	OT(3)	OT(4)
$CHCl_3$ (mL)	64	32	32	16
Toluene (mL)	0	32	32	48
Temperature (°C)	55	55	85	85

2.3. Synthesis of water soluble nanoparticles

5 mg powder of OT coated gold NPs were dissolved in 10 mL $CHCl_3$. 10 mg of MUS ligand was dissolved in 10 mL methanol and added to the NP solution. The ligand exchange reaction was stirred overnight to obtain approximately 2:1 MUS:OT ratio. The resulting NPs were collected with centrifugation under 5000 g and 15 min followed by dissolving in 15 mL water. Then, water soluble NPs were thoroughly washed with Amicon® centrifugal filters (30 kDa MWCO) and concentrated into final 0.5 mL solution which was used as stock solution for the protein incubation experiments.

In order to obtain MUS:OT 8:1 NPs, the starting MUS ligand for the exchange was increased to 40 mg while keeping the OT NPs amount constant. Also, the reaction was heated to 50 °C for at least 1 h to increase the kinetics and favor ligand exchange to higher ratios. As the solvent evaporated from the reaction flask, methanol was added to prevent drying the reaction solution. Finally, the NPs were cooled down to room temperature and methanol was added to initiate precipitation. NPs were collected *via* centrifugation (5000 g for 15 min) and dissolved again in water. The NP solution was then washed repeatedly with Amicon® centrifugal filters (30 kDa MWCO) and concentrated down to 0.5 mL which was stored as stock solution.

2.4. Protein – NP titration experiments

Approximately 5–6 mg of human serum albumin (HSA) was dissolved in 1 mL 10 mM phosphate buffer (pH 7.4). This protein solution was diluted to half concentration sequentially for at least 15 times in order to reach 10^{-7} to 10^{-8} M range in 0.5 mL. Then, gold NPs were added to each of these solutions separately and incubated for at least 24 h at 4 °C.

2.5. AUC experiments

All AUC experiments were carried out in aluminum coated AUC cell holder with Epon® centerpiece and sapphire windows. The AUC rotor was pre-chilled to 20 °C for at least 1 h prior to centrifugation. Sedimentation velocity AUC experiments were carried out in absorbance mode at 520 nm with 0.006 cm scan rate to keep track of only gold NPs sedimentation. All of the sedimentation data was analyzed with free software SEDFIT which was obtained from www.analyticalultracentrifugation.com. Hydrodynamic diameter (d_{hyd}) and hydrodynamic density (ρ_{NP}) of gold NPs were calculated using previously reported protocol employing a custom made Matlab script [26]. Sedimentation (s) and diffusion coefficients (D) were primarily used to

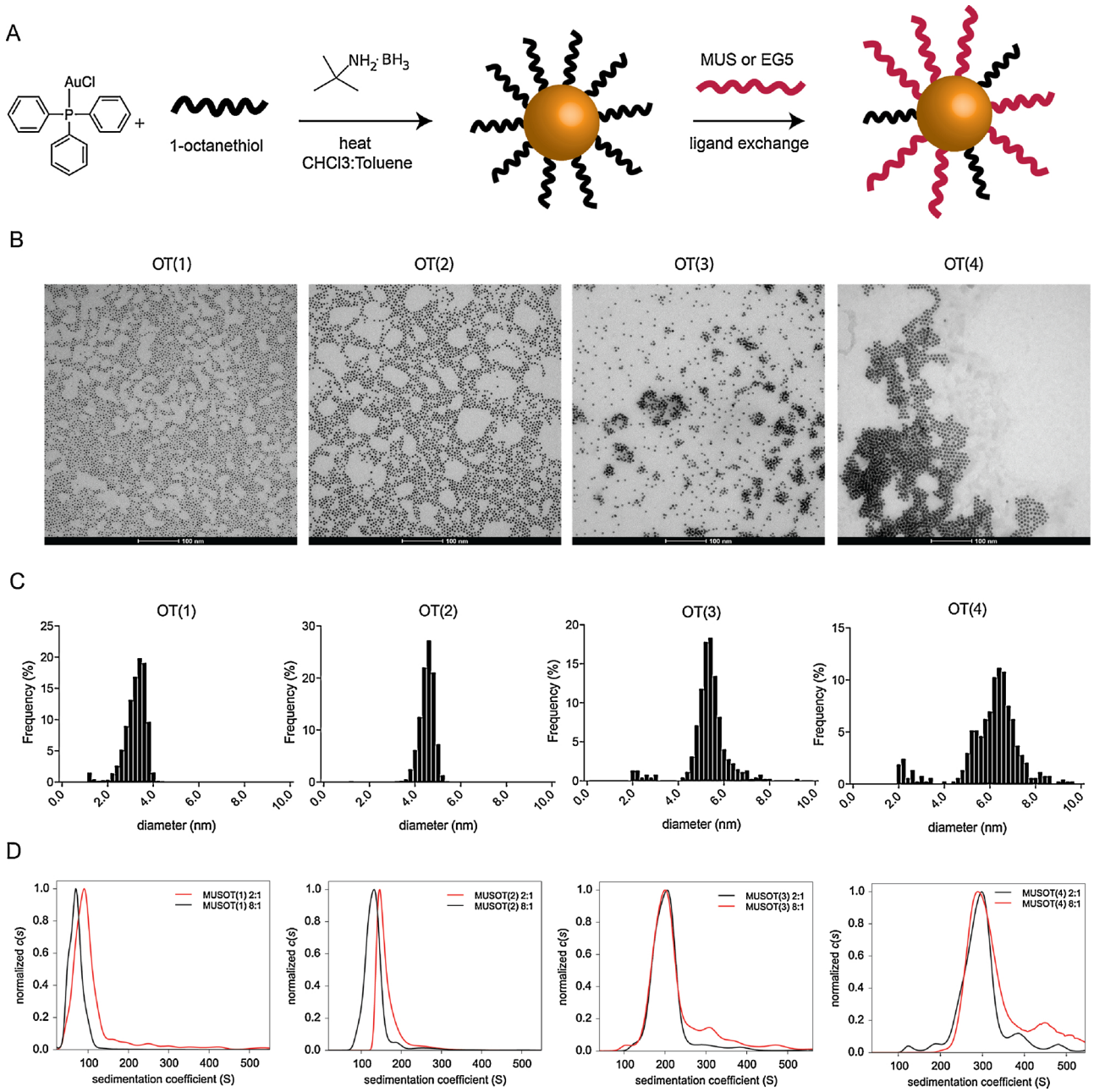

Fig. 1. A) Schematic representation of the synthetic protocol followed for all NPs used in this work. B) Representative electron microscopy images for each size of OT coated gold NPs. Scale bar is 100 nm in each images. C) Size histograms obtained from multiple TEM images (> 2000 NPs). D) Sedimentation coefficient distribution of each size of NPs with 2:1 and 8:1 MUS:OT ratio. Note that while size (3) and (4) have similar distribution for both type of NPs, (1) and (2) are different as the effect of hydrophobic OT becomes more significant on the colloidal stability of the NPs and their size becomes smaller due to the smaller number of water-stabilizing hydrophilic ligands present on the smaller NPs.

calculate d_{hyd} and ρ_{NP}, however, unlike the reference, frictional ratio was not assumed to be 1 for all NPs. In order to make AUC analysis for protein – NP interactions, NP density was calculated *via* hard-sphere model where hydration layer is removed for the sake of physical relevance of the binding event [23].

3. Results and discussion

3.1. Design and synthesis of gold nanoparticles

We synthesized 4 different size of gold NPs *via* controlled reduction of organic soluble gold triphenylphosphine salts with borane containing mild reducing agents (Fig. 1A) [27]. The advantage of this method lies in the ability to control efficiently the size of resulting gold NPs by changing solely the reaction temperature and solvent polarity. For example, using chloroform as the only solvent at 55 °C resulted in nanoparticles of approximately 3–4 nm core diameter, when the temperature was increased to 85 °C and a mixture of 1:1 chloroform:toluene was used, the reaction product were gold NPs approximately 5–6 nm in core diameter (Table 1). Keeping all the other reaction parameters constant, this method allowed us to produce gold NPs with different sizes in a consistent and reliable way. It is worth stressing the importance of not changing synthetic parameters such as starting gold salt material or type of reducing agent because these factors can influence the quality of the NPs or introduce possible contaminants. For the same reasons, we used only 1-octanethiol (OT) as the starting ligand on the surface of

Table 2
Hydrodynamic analysis of NPs as a result of combined TEM and AUC measurements. Standard deviations are measured as one σ value of the sedimentation and diffusion distribution obtained from AUC and TEM size histogram.

	s (10^{-13} s)	D (10^{-11} m^2s^{-1})	ρ_{NP} (gcm^{-3})	d_{hyd} (nm)	d_{core} (nm)
MUSOT(1) 8:1	68 ± 16	6.5 ± 0.9	4.6 ± 0.9	6.5 ± 0.8	3.2 ± 0.5
MUSOT(2) 8:1	123 ± 22	6.1 ± 0.8	5.7 ± 0.7	7.6 ± 0.9	4.5 ± 0.7
MUSOT(3) 8:1	214 ± 35	5.3 ± 0.7	7.0 ± 0.8	8.8 ± 0.7	5.6 ± 0.6
MUSOT(4) 8:1	296 ± 43	4.9 ± 0.8	8.2 ± 1.1	10.4 ± 0.7	6.6 ± 0.6
MUSOT(1) 2:1	95 ± 21	5.6 ± 0.8	3.9 ± 0.6	7.6 ± 0.6	3.2 ± 0.5
MUSOT(2) 2:1	155 ± 27	5.3 ± 0.7	5.3 ± 0.4	8.1 ± 0.7	4.5 ± 0.7
MUSOT(3) 2:1	213 ± 33	5.8 ± 0.7	8.0 ± 0.6	8.2 ± 0.7	5.6 ± 0.6
MUSOT(4) 2:1	294 ± 47	5.3 ± 0.6	9.2 ± 0.7	9.5 ± 0.8	6.6 ± 0.6

gold NPs during synthesis and produced all of the water-soluble NPs directly from OT coated gold NPs. As a secondary step, we introduced 11-mercaptoundecane sulfonate (MUS) through ligand exchange reactions with stoichiometric ratios of either 2:1 MUS:OT or 8:1 MUS:OT. We chose these two compositions as the 2:1 has been shown to have a ligand shell with stripe-like domains [20,28], while the 8:1 being mostly a homoligand NPs should present a homogeneous distribution of ligands [29,30]. We were not able to produce truly homoligand particles through this synthetic route as MUS is a highly charged molecule, and this limits the progress of ligand exchange particularly at higher MUS:OT ratios possibly due to increasing effect of repulsion upon MUS crowding. Nonetheless, given the low amount of OT in MUS:OT 8:1 NPs, we expect the influence of OT on protein binding would be minimum and the NPs would behave similar to fully MUS coated NPs (Figure S1 and S2). Similarly, a third type of NPs was synthesized *via* ligand exchange of HS-EG5-OH (EG5) from OT coated NPs. Although they also have a slight amount of OT residuals on the surface, they are low enough to consider these NPs almost fully coated with EG5.

After synthesis, all of the NPs in this work were thoroughly characterized with TEM and AUC for determination of the core (d_{core}) and the hydrodynamic diameter (d_{hyd}) respectively (Fig. 1B and 1C). NPs that had similar core size were denoted with the same numbering in the parenthesis from 1 to 4 with 1 being the smallest to 4 being the largest (*i.e.* d_{core}\{MUSOT(1)\} < d_{core}\{MUSOT(2)\}, d_{core}\{MUSOT(3)\} < d_{core}\{MUSOT(4)\},). According to the AUC method described previously [26], we were able to calculate d_{hyd} of NPs as well as hydrodynamic density (ρ_{NP}) based on their sedimentation coefficients (s) and diffusion coefficients (D). Interestingly, MUSOT(1) and MUSOT(2) NPs showed disparity in average sedimentation coefficient values between 2:1 and 8:1 ligand mixture whereas MUSOT(3) and MUSOT(4) had almost identical sedimentation coefficient distributions (Fig. 1D). This suggests that binary ligand mixture might not be distributed homogeneously over the NP surface for all sizes particularly when d_{core} becomes smaller than 5 nm. Subsequently, with the help of the diffusion coefficient obtained from AUC, we were able to calculate ρ_{NP} for all the NPs (Table 2). According to the results, ρ_{NP} of MUSOT 8:1 was found smaller than MUSOT 2:1 NPs for size (3) and (4) NPs. This, in fact, was expected considering the lower amount of sulfonate ligands on 2:1 NPs compared to the 8:1NPs, resulting in a decreased hydration layer and thus an increased ρ_{NP}. However, the same behavior was not observed for size (1) and (2) NPs. That is, for example, ρ_{NP} of MUSOT(1) 2:1 was considerably smaller than that of MUSOT(1) 8:1. These findings highlight that MUSOT(1) 2:1 and MUSOT(2) 2:1 could potentially have inhomogeneous hydration layers around the surface due to locally concentrated sulfonate ligands. In fact, these NPs previously were shown to exhibit surface structures that affected their colloidal stability through non-conventional hydration [31].

3.2. Protein – nanoparticle interaction thermodynamics

After the synthesis of these monodisperse NPs, we titrated each NPs with varying concentrations of human serum albumin (HSA) in 10 mM phosphate buffer pH 7.4 while keeping the NP concentration constant. Each titration mixture was then centrifuged in AUC to determine average s-value distribution of the corresponding NP – HSA complex. Upon protein adsorption, sedimentation of gold NPs is observed to slow down due to 'the parachute effect' (Fig. 2A). Subsequently, we modelled the gradual decrease of the sedimentation by incorporating the Hill formulation into the Svedberg equation which resulted the following description [23]:

$$s_{cx}([HSA]) = \frac{2}{9\eta}\sqrt[3]{\frac{9}{16\pi}}\frac{(\rho_{NP}-\rho_s)V_{NP}+N_{max}\frac{1}{1+\left(K_D/[HSA]\right)^n}(\rho_P-\rho_s)V_P}{\left(V_{NP}+N_{max}\frac{1}{1+\left(K_D/[HSA]\right)^n}V_P\right)^{1/3}} \quad (1)$$

where ρ_{NP}, ρ_P and V_{NP}, V_P are density of NP and protein, and volume of NP and protein respectively. These fixed parameters were calculated for each NP and protein mixture separately by following the hard sphere model [23]. For all NPs, three separate titration sets were performed with identical conditions (incubation temperature, buffer solutions, *etc.*) and resulting s-values were averaged across the three values together with the calculation of standard deviations as error bars (Fig. 2B). The combination of s-values of each NP – HSA complexes (s_{cx}) forms a Langmuir-type of adsorption isotherm which was then fitted to the equation 1 with root mean square deviation protocol (Fig. 2B). The result of the fit allowed us to calculate binding affinity (K_D), stoichiometry (N_{max}) as well as cooperativity (Hill coefficient (n). The variance of the values is defined as the root mean square error and regarded as the error bars in the following plots (Figure S3 and S4).

Following this method, we calculated the K_D and N_{max} values for all MUSOT 2:1 and 8:1 NPs (Fig. 3). According to these results, for MUSOT 8:1 NPs, there is a linear trend on K_D values with respect to surface area (hence, a quadratic relation with the NP size) which was calculated by radius of gold core plus the size of ligands in full extension (Fig. 3). The increase of K_D as the size decreases indicate weaker binding of small NPs to HSA. Similarly, previously published reports on ultrasmall gold nanoparticles demonstrated that the protein interactions can diminish as the size gets smaller which could eventually evade forming protein corona [17]. For HSA binding to MUSOT 2:1 NPs, such linearity slightly decreased but was found to be statistically significant ($R^2 = 0.91$) indicating that the presence of binary ligands does not dramatically change the monotonic relation of size and binding affinity. Additionally, most of the 2:1 mixed-ligand NPs exhibit slightly lower K_D values than their 8:1 equivalents, therefore, have higher affinity to HSA binding. This can be explained by the preferential binding of albumins to hydrophobic molecules which is their one of the primary functions in blood [32]. In short, our results show that binding affinity is clearly a function of size where a monotonic decrease is observed as the size of NPs get smaller.

The number of proteins bound to MUSOT 8:1 and 2:1 exhibited a higher disparity according to the AUC analysis (Fig. 3). In parallel to K_D values, MUSOT 8:1 NPs showed a linear trend with NP surface area such that small NPs accommodate fewer proteins on the surface

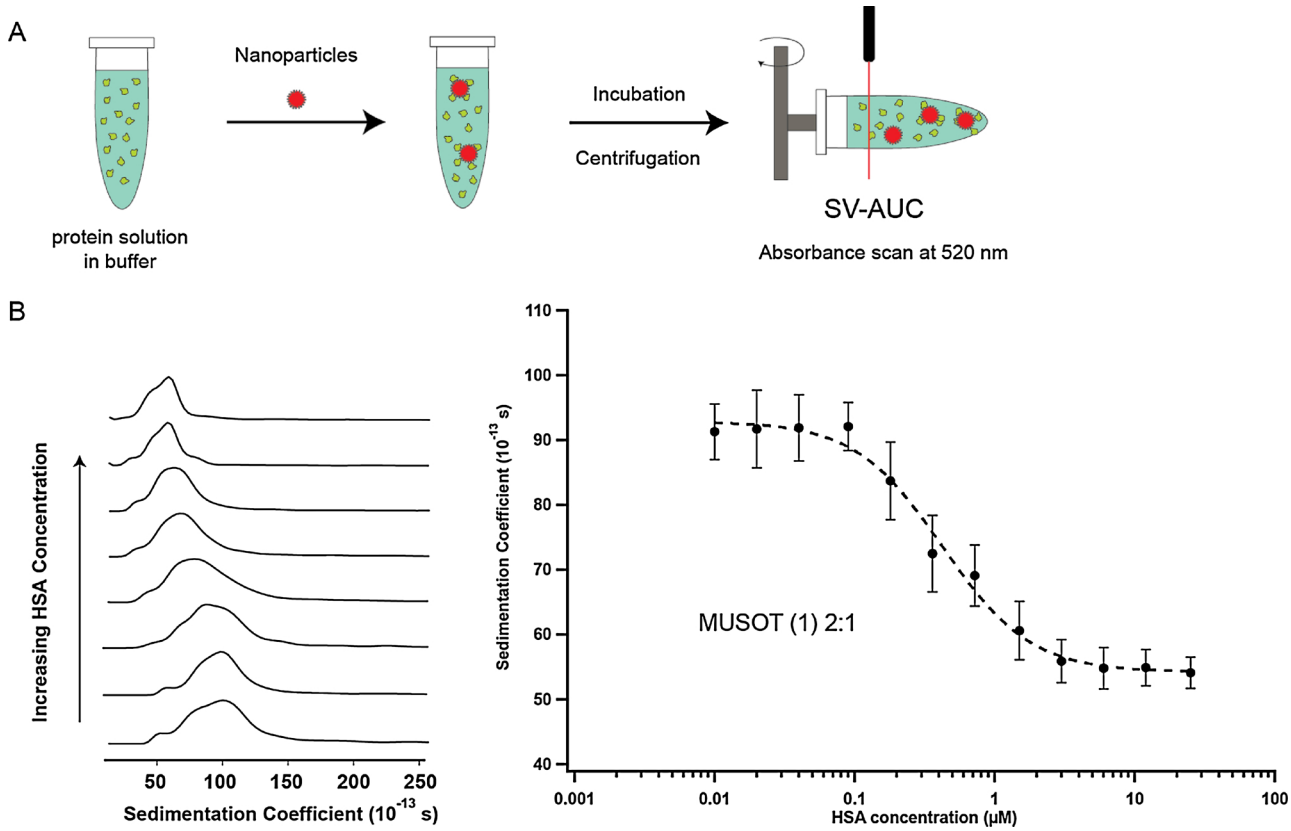

Fig. 2. A) Schematic drawing of the AUC experiments performed to determine NP/protein binding thermodynamics. NPs were put in varying concentrations of HSA solution, incubated overnight and centrifuged down in the Epon centerpiece of AUC. B) A gradual shift of sedimentation distribution of NP upon increasing HSA concentration was clearly observed for example in the MUSOT(1) 2:1 NPs. When average *s*-values were plotted against protein amount, a sigmoidal decrease could be fitted to Eq. (1) and the binding parameters, K_D and N_{max}, were calculated. Error bars represent the standard deviation over the average of three replicate measurements of NPs/HSA mixtures in separate vials.

compared to larger NPs. Considering the available surface area increases for protein binding across homogeneous surface coatings in these NPs, the monotonic behavior was somewhat anticipated. In fact, similar behavior has also been observed for much larger NPs (> 100 nm) [33]. On the other hand, MUSOT 2:1 NPs do not fit into this model with a non-monotonic behavior for N_{max} values of HSA binding. In addition, MUSOT 2:1 (1) and MUSOT 2:1 (2) NPs seemingly interact with slightly more HSA molecules when compared to same size of 8:1 NPs. As seen in the binding affinity case, the presence of hydrophobic residues on mixed ligand NPs might have resulted in such discrepancy. However, larger MUSOT NPs show a dramatic decrease in N_{max} values suggesting that other factors such as the surface morphology could be taking part as well. The decreased number of bound protein for these NPs could also be the result of disparate binding orientation of HSA on the structured amphiphilic ligand shell of gold NPs [18]. In essence, these findings recapitulate how surface heterogeneity at the nano-level could impact the NPs behavior and demonstrate that thermodynamics of NP/protein interactions are not exceptions as well.

3.3. Ethylene glycol NPs

The third set of NPs we prepared was ethylene glycol (EG5) coated gold NPs with similar core diameters. AUC analysis with our model protein HSA was carried out for different sized EG5 NPs with the aim of obtaining K_D and N_{max} values similar to MUSOT NPs (Fig. 4A). However, even with an increased range of protein concentration up to 1 mM, we did not find any decrease in the average sedimentation coefficient upon protein attachment (Fig. 4B). This implies that dissociation constant (K_D) of HSA from EG5 NPs is immeasurably high (more than 1 mM) and thus the interaction between EG5 NPs and HSA is extremely weak. All of the sizes we tested in this work demonstrated the same behavior and therefore we could not make any distinction on their size dependency and binding affinity. However, with these studies we confirmed that incorporation of ethylene glycol units to NP ligand shell inferred protein resistance to NPs and therefore they can evade from attaching proteins in parallel to previous works by others [34]. For the context of the protein corona, on the other hand, complex media such as human serum should be used to reach to more general conclusions.

4. Conclusions and outlook

NPs have important physicochemical parameters that can potentially affect the protein binding behavior and as a result the final protein corona. Several studies tried to investigate the effect of these parameters but almost exclusively for very large NPs that have several hundred nanometers in core diameters. Here, we have reported a systematic study of sub-10 nm gold NPs and their binding behavior towards our model protein human serum albumin. Our study exclusively utilized recently developed AUC based method for high quality determination of binding affinity and stoichiometry for these small NPs. For both 8:1 and 2:1 gold NPs, we found that binding affinity of HSA tend to follow a linear trend, albeit in a slightly different manner, with respect to NP surface area. However, in terms of maximum protein coverage on NP surface, we found that a linear trend was present solely for the 8:1 NPs whereas no discernible trend could be found for the 2:1 NPs. This irregular protein binding behavior for 2:1 NPs was attributed to the patchy character of surface ligands which potentially influences NP/protein binding configuration.

Finally, we have investigated the effect of small ethylene glycol units incorporated to gold NPs which resulted in almost complete

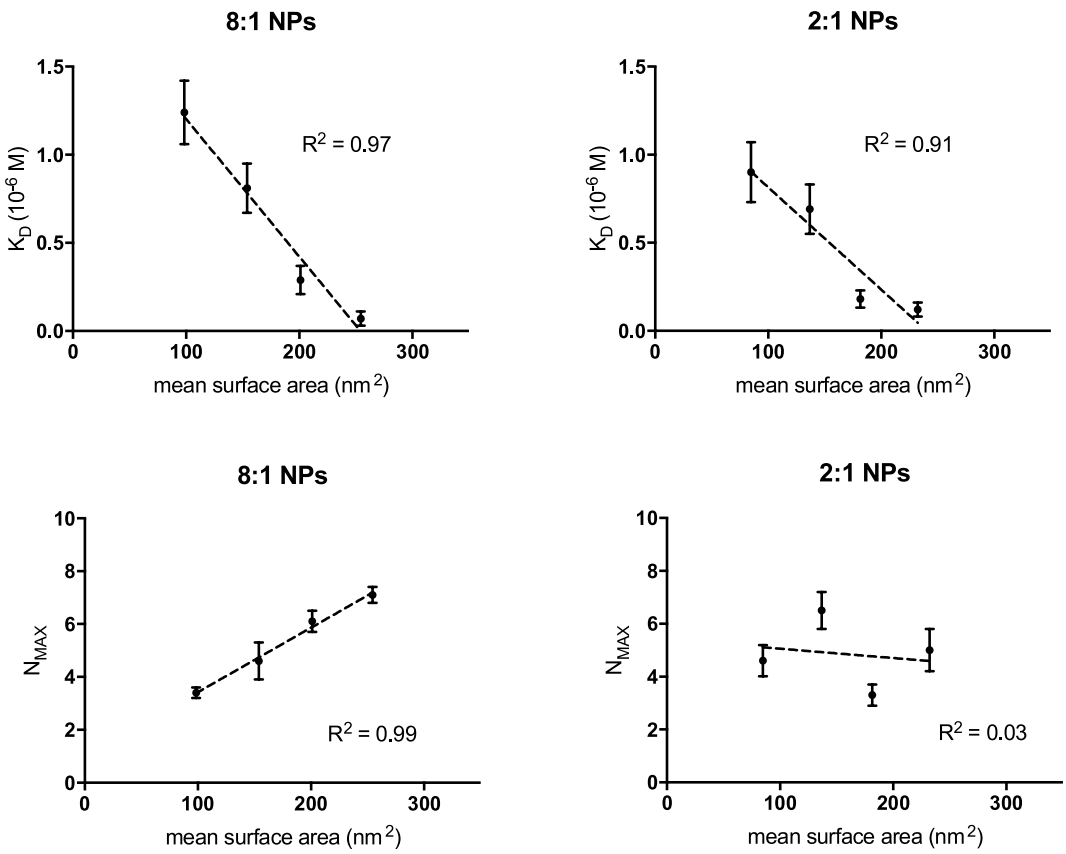

Fig. 3. NPs/HSA binding parameters plotted with respect to average surface area of NPs. The linear relationship was observed for 8:1 NPs whereas 2:1 NPs tend to behave irregularly particularly for N_{max} values. The error bars represent the root-mean-square deviation calculated by sigmoidal curve fit of Eq. (1).

resistance to HSA attachment. These results confirmed the effect of PEGylation on protein binding but shown for the first time for sub-10 nm NPs. Overall, this study sheds light on the size and surface structure effect on protein binding thermodynamics for sub-10 nm gold NPs.

Characterization of thermodynamic aspects of protein interactions with NPs is a key factor to fully understanding protein corona and designing more efficient nanomaterials for therapy as well as diagnostics. The physicochemical studies such as we report here not only contribute to this aim but also serve as crucial steps toward building more sophisticated NP/protein systems that recapitulate more relevant *in vivo* conditions. The next big challenge will be to build models that are able to take in multi-protein/multi-nanoparticle systems at least at equilibrium. We believe that AUC based interaction methods could be reformulated by taking into account multiple proteins' sedimentation coefficients and calculating the bound/unbound protein numbers *via* estimating the area under the sedimentation distributions. This could, in principle, also be extrapolated towards using multiple NP sizes in one batch and investigating their protein interactions.

As one of the most promising features of nanomedicine is the ability

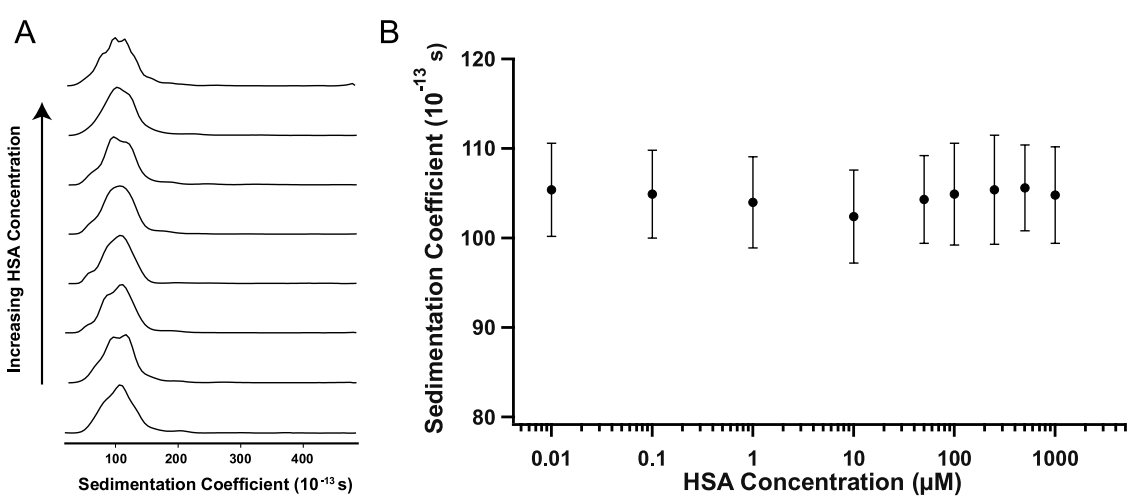

Fig. 4. A) The overlay of *s*-value distributions of EG5/HSA mixtures and B) average *s*-values for each mixing points. Even after mixing with 1 mM of HSA, EG5 NPs do not change in sedimentation behavior, implying that the interaction with the protein is lacking. Error bars represent the average of three replicate measurements of EG5/HSA mixture in separate vials.

to tune NP properties to design smart medical tools, such systematic studies would reveal which NP formulations would result in structural perturbations in protein structure as well as how dense protein corona would occur on NP surface for certain NP/protein mixtures. These, in fact, have been shown to significantly influence the targeting efficiency of NPs as well as their stability in blood and as a result, clearance rate by the reticuloendothelial system [35,36]. In addition, these studies would enable to 'manually' design protein corona systems to improve the impact and availability of nanomaterials *in vivo* [37,38].

Acknowledgments

This article is dedicated to the retirement of Prof. Heinrich Hofmann (LTP, EPFL, Switzerland) a key figure in nano-bio interactions. The Swiss National Science Foundation is gratefully acknowledged for a Division II funding.

Appendix A. Supplementary data

Supplementary material related to this article can be found, in the online version, at doi:https://doi.org/10.1016/j.colsurfb.2018.11.027.

References

[1] D. Bonvin, U. Aschauer, D.T.L. Alexander, D. Chiappe, M. Moniatte, H. Hofmann, et al., Protein corona: impact of lymph versus blood in a complex in vitro environment, Small 13 (2017) 1700409, , https://doi.org/10.1002/smll.201700409.
[2] M. Hofmann-Amtenbrink, D.W. Grainger, H. Hofmann, Nanoparticles in medicine: current challenges facing inorganic nanoparticle toxicity assessments and standardizations, Nanomedicine 11 (2015) 1689–1694, https://doi.org/10.1016/j.nano.2015.05.005.
[3] K. Choi, J.E. Riviere, N.A. Monteiro-Riviere, Protein corona modulation of hepatocyte uptake and molecular mechanisms of gold nanoparticle toxicity, Nanotoxicology 11 (2017) 64–75, https://doi.org/10.1080/17435390.2016.1264638.
[4] C.D. Walkey, J.B. Olsen, F. Song, R. Liu, H. Guo, D.W.H. Olsen, et al., Protein corona fingerprinting predicts the cellular interaction of gold and silver nanoparticles, ACS Nano 8 (2014) 2439–2455, https://doi.org/10.1021/nn406018q.
[5] V. Mirshafiee, M. Mahmoudi, K. Lou, J. Cheng, M.L. Kraft, Protein corona significantly reduces active targeting yield, Chem. Commun. 49 (2013) 2557–2559, https://doi.org/10.1039/c3cc37307j.
[6] G. Caracciolo, O.C. Farokhzad, M. Mahmoudi, Biological identity of nanoparticles in vivo: clinical implications of the protein corona, Trends Biotechnol. 35 (2017) 257–264, https://doi.org/10.1016/j.tibtech.2016.08.011.
[7] A.E. Nel, L. Mädler, D. Velegol, T. Xia, E.M.V. Hoek, P. Somasundaran, et al., Understanding biophysicochemical interactions at the nano–bio interface, Nat. Mater. 8 (2009) 543–557, https://doi.org/10.1038/nmat2442.
[8] S. Tenzer, D. Docter, J. Kuharev, A. Musyanovych, V. Fetz, R. Hecht, et al., Rapid formation of plasma protein corona critically affects nanoparticle pathophysiology, Nat. Nanotech. 8 (2013) 772–781, https://doi.org/10.1038/nnano.2013.181.
[9] C.D. Walkey, J.B. Olsen, H. Guo, A. Emili, W.C.W. Chan, Nanoparticle size and surface chemistry determine serum protein adsorption and macrophage uptake, J. Am. Chem. Soc. 134 (2012) 2139–2147, https://doi.org/10.1021/ja2084338.
[10] S. Tenzer, C. Bier, A. Wlodarski, W. Mann, S. Rosfa, H. Schild, et al., Nanoparticle size is a critical physicochemical determinant of the human blood plasma corona: a comprehensive quantitative proteomic analysis, ACS Nano 5 (2011) 7155–7167, https://doi.org/10.1021/nn201950e.
[11] U. Sakulkhu, M. Mahmoudi, L. Maurizi, J. Salaklang, H. Hofmann, Protein corona composition of superparamagnetic iron oxide nanoparticles with various physicochemical properties and coatings, Sci. Rep. 4 (2014) 5020, https://doi.org/10.1038/srep05020.
[12] U. Sakulkhu, L. Maurizi, M. Mahmoudi, M. Motazacker, M. Vries, A. Gramoun, et al., Ex situ evaluation of the composition of protein corona of intravenously injected superparamagnetic nanoparticles in rats, Nanoscale 6 (2014) 11439–11450, https://doi.org/10.1039/C4NR02793K.
[13] D. Bonvin, D. Chiappe, M. Moniatte, H. Hofmann, M. Mionić Ebersold, Methods of protein corona isolation for magnetic nanoparticles, Analyst 142 (2017) 3805–3815, https://doi.org/10.1039/c7an00646b.
[14] U. Sakulkhu, M. Mahmoudi, L. Maurizi, G. Coullerez, M. Hofmann-Amtenbrink, M. Vries, et al., Significance of surface charge and shell material of superparamagnetic iron oxide nanoparticle (SPION) based core/shell nanoparticles on the composition of the protein corona, Biomater. Sci. 3 (2015) 265–278, https://doi.org/10.1039/C4BM00264D.
[15] S.H.D.P. Lacerda, J.J. Park, C. Meuse, D. Pristinski, M.L. Becker, A. Karim, et al., Interaction of gold nanoparticles with common human blood proteins, ACS Nano 4 (2010) 365–379, https://doi.org/10.1021/nn9011187.
[16] T. Cedervall, I. Lynch, M. Foy, T. Berggård, S.C. Donnelly, G. Cagney, et al., Detailed identification of plasma proteins adsorbed on copolymer nanoparticles, Angew. Chem. Int. Ed. Engl. 46 (2007) 5754–5756, https://doi.org/10.1002/anie.200700465.
[17] L. Boselli, E. Polo, V. Castagnola, K.A. Dawson, Regimes of biomolecular ultrasmall nanoparticle interactions, Angew. Chem. Int. Ed. Engl. 56 (2017) 4215–4218, https://doi.org/10.1002/anie.201700343.
[18] R. Huang, R.P. Carney, K. Ikuma, F. Stellacci, B. Lau, Effects of surface compositional and structural heterogeneity on nanoparticle–protein interactions: different protein configurations, ACS Nano 8 (2014) 5402–5412, https://doi.org/10.1021/nn501203k.
[19] A.M. Jackson, J.W. Myerson, F. Stellacci, Spontaneous assembly of subnanometre-ordered domains in the ligand shell of monolayer-protected nanoparticles, Nat. Mater. 3 (2004) 330–336, https://doi.org/10.1038/nmat1116.
[20] R.P. Carney, G.A. DeVries, C. Dubois, H. Kim, J.Y. Kim, C. Singh, et al., Size limitations for the formation of ordered striped nanoparticles, J. Am. Chem. Soc. 130 (2008) 798–799, https://doi.org/10.1021/ja077383m.
[21] A. Verma, O. Uzun, Y. Hu, Y. Hu, Y. Hu, H.-S. Han, et al., Surface-structure-regulated cell-membrane penetration by monolayer-protected nanoparticles, Nat. Mater. 7 (2008) 588–595, https://doi.org/10.1038/nmat2202.
[22] A. Verma, F. Stellacci, Effect of surface properties on nanoparticle-cell interactions, Small 6 (2010) 12–21, https://doi.org/10.1002/smll.200901158.
[23] A. Bekdemir, F. Stellacci, A centrifugation-based physicochemical characterization method for the interaction between proteins and nanoparticles, Nat. Commun. 7 (2016) 13121, https://doi.org/10.1038/ncomms13121.
[24] C. Röcker, M. Pötzl, F. Zhang, W.J. Parak, G.U. Nienhaus, A quantitative fluorescence study of protein monolayer formation on colloidal nanoparticles, Nat. Nanotechnol. 4 (2009) 577–580, https://doi.org/10.1038/nnano.2009.195.
[25] R.C. Van Lehn, M. Ricci, P.H.J. Silva, P. Andreozzi, J. Reguera, K. Voïtchovsky, et al., Lipid tail protrusions mediate the insertion of nanoparticles into model cell membranes, Nat. Commun. 5 (2014) 4482, https://doi.org/10.1038/ncomms5482.
[26] R.P. Carney, J.Y. Kim, H. Qian, R. Jin, H. Mehenni, F. Stellacci, et al., Determination of nanoparticle size distribution together with density or molecular weight by 2D analytical ultracentrifugation, Nat. Commun. 2 (2011) 335, https://doi.org/10.1038/ncomms1338.
[27] G.D. Stucky, N. Zheng, J. Fan, One-step one-phase synthesis of monodisperse noble-metallic nanoparticles and their colloidal crystals, J. Am. Chem. Soc. 128 (2006) 6550–6551, https://doi.org/10.1021/ja0604717.
[28] G.A. DeVries, M. Brunnbauer, Y. Hu, A.M. Jackson, B. Long, B.T. Neltner, et al., Divalent metal nanoparticles, Science 315 (2007) 358–361, https://doi.org/10.1126/science.1133162.
[29] M. Şologan, D. Marson, S. Polizzi, P. Pengo, S. Boccardo, S. Pricl, et al., Patchy and janus nanoparticles by self-organization of mixtures of fluorinated and hydrogenated alkanethiolates on the surface of a gold core, ACS Nano 10 (2016) 9316–9325, https://doi.org/10.1021/acsnano.6b03931.
[30] P.K. Ghorai, S.C. Glotzer, Atomistic simulation study of striped phase separation in mixed-ligand self-assembled monolayer coated nanoparticles, J. Phys. Chem. C 114 (2010) 19182–19187, https://doi.org/10.1021/jp105013k.
[31] R. Huang, R.P. Carney, F. Stellacci, B.L.T. Lau, Colloidal stability of self-assembled monolayer-coated gold nanoparticles: the effects of surface compositional and structural heterogeneity, Langmuir 29 (2013) 11560–11566, https://doi.org/10.1021/la4020674.
[32] M. Fasano, S. Curry, E. Terreno, M. Galliano, G. Fanali, P. Narciso, et al., The extraordinary ligand binding properties of human serum albumin, IUBMB Life 57 (2005) 787–796, https://doi.org/10.1080/15216540500404093.
[33] S. Lindman, I. Lynch, E. Thulin, H. Nilsson, K.A. Dawson, S. Linse, Systematic investigation of the thermodynamics of HSA adsorption to N-iso-Propylacrylamide/N-tert-butylacrylamide copolymer nanoparticles. Effects of particle size and hydrophobicity, Nano Lett. 7 (2007) 914–920, https://doi.org/10.1021/nl062743.
[34] Q. Dai, C. Walkey, W.C.W. Chan, Polyethylene glycol backfilling mitigates the negative impact of the protein corona on nanoparticle cell targeting, Angew. Chem. Int. Ed. Engl. 53 (2014) 5093–5096, https://doi.org/10.1002/anie.201309464.
[35] N. Bertrand, P. Grenier, M. Mahmoudi, E.M. Lima, E.A. Appel, F. Dormont, et al., Mechanistic understanding of in vivo protein corona formation on polymeric nanoparticles and impact on pharmacokinetics, Nat. Commun. 8 (2017) 777, https://doi.org/10.1038/s41467-017-00600-w.
[36] S. Schöttler, K. Landfester, V. Mailänder, Controlling the stealth effect of nanocarriers through understanding the protein corona, Angew. Chem. Int. Ed. Engl. 55 (2016) 8806–8815, https://doi.org/10.1002/anie.201602233.
[37] J.Y. Oh, H.S. Kim, L. Palanikumar, E.M. Go, B. Jana, S.A. Park, et al., Cloaking nanoparticles with protein corona shield for targeted drug delivery, Nat. Commun. 9 (2018) 2780, https://doi.org/10.1038/s41467-018-06979-4.
[38] J. Guan, Q. Shen, Z. Zhang, Z. Jiang, Y. Yang, M. Lou, et al., Enhanced immunocompatibility of ligand-targeted liposomes by attenuating natural IgM absorption, Nat. Commun. 9 (2018) 36, https://doi.org/10.1038/s41467-018-05384-1.